Electronic Supplementary Information

Mo-P Sites Boosting Interfacial Charge Transfer of 2D/3D MoS_2/TiO_2 Heterostructure for Efficient Photocatalytic Hydrogen Evolution and Chromium (VI) Reduction

Yaoyao Wu,[a*] Jiachun Cao,[b] Ruihao Peng,[a] Miao Cao,[a] Guan Peng,[c] Wenjing Yuan,[c] Xianping Luo,[a,*]

[a] *Jiangxi Provincial Key Laboratory of Environmental Pollution Prevention and Control in Mining and Metallurgy, School of Resources and Environmental Engineering, Jiangxi University of Science and Technology, Ganzhou 341000, China*

[b] *Institute of Environmental Health and Pollution Control, School of Environmental Science and Engineering, Guangdong University of Technology, Guangzhou 510006, PR China*

[c] *Ganjiang Innovation Academy, Chinese Academy of Sciences, Ganzhou 341119, China*

* Corresponding authors: Yaoyao Wu, E-mail: wuyy6@jxust.edu.cn; Xianping Luo, E-mail: luoxianping@jxust.edu.cn

Content

This file contains 27 pages, 5 texts, 16 figures and 4 tables.

Supplementary Materials Include:

Text S1. Synthesis of materials

1.1. Synthesis of TiO_2 HM

TiO_2 HM was prepared using the simple solvothermal and annealing approach. N, N-dimethylformamide (15 mL) was stirred with triethanolamine (30 mL). Then, titanium isopropoxide (1.5 mL) was injected to the mixed solution for half an hour while stirring. The mixture was transferred to an autoclave and then kept 200 °C for 24 h. The white precipitates were rinsed with deionized water and ethanol for three times and dried in air. Further, the obtained samples were calcinated in air at a ramp rate of 10 °C min^{-1} for 2 h and maintained at 500 °C for another 2 h in a muffle furnace.[1]

1.2. Synthesis of MoS_2

The MoS_2 were synthesized through a one-step hydrothermal route with $(NH_4)_2MoS_4$ as the precursor. In a typical procedure, $(NH_4)_2MoS_4$ (0.1 mol) was dispersed in 30 mL of deionized water. After ultrasonication for half an hour, the mixture was transferred to an autoclave and kept at 200 °C for 10 h. The obtained precipitate was rinsed with deionized water and ethanol for three times, and dried at 60 °C for overnight.

Text S2. Photocatalytic H_2 production activity

The photocatalytic H_2 production reaction was performed in a vacuum system with 300 W Xe lamp (CeAuLight) as a simulated solar light source. Photocatalyst powder (25 mg) was suspended in 100 mL solution containing triethanolamine (20 mL) as a sacrificial agent. The above mixture was fully degassed and H_2 evolution rate was measured by online gas chromatography (CG1690, TCD). The recyclability of P-MoS_2/TiO_2 HM was evaluated by repeating the photocatalytic reaction for four cycles

with 5 h intervals.

Text S3. Photocatalytic Cr (VI) removal

Photocatalyst powder (25 mg) was dispersed in a solution with an initial concentration of 8 mg L^{-1} of $K_2Cr_2O_7$. The pH was adjusted to 3 using dilute sulfuric acid. The mixture was stirred in the dark for 0.5 h to achieve equilibrium between adsorption and desorption. Subsequently, the suspension was irradiated with a 300 W Xenon lamp. At specific time intervals, samples were filtered using a 0.22 μm filter, and the concentration of Cr (VI) ions was determined using a UV-visible spectrophotometer and the colorimetric method.

Text S4. Characterization and electrochemical tests

4.1. Electrochemical tests

Electrochemical measurements were conducted at a Gamry Reference 3000 electrochemical workstation (USA). The photocurrents, steady-state linear sweep voltammetry (LSV) curves, electrochemical impedance spectroscopy (EIS) and Mott-Schottky measurements were carried out in a standard three-electrode cell containing Na_2SO_4 (0.1 M) aqueous solution with a Pt plate and an Ag/AgCl electrode as the counter and reference electrode, respectively. The detailed preparation procedures of working electrodes were as follow: the fluorine doped tin oxide glass was ultrasonically cleaned in distilled water and isopropanol for half an hour sequentially. The catalyst (5 mg) was ultrasonically dispersed in an ethanol solution (1 mL) for half an hour. Then, the mixture (500 μL) was dispersed onto the FTO substrate as working electrode. The resulting film was dried in air, yielding an electrode with catalyst loading amount of ca.

0.5 mg cm^{-1}. The photocurrents were measured under 300 W Xe lamp irradiation.

4.2. Characterization

The morphology was observed by field-emission scanning electron microscopy (FESEM; ZEISS, Sigma 500). Transmission electron microscopy (TEM) images, high-resolution TEM (HR-TEM) analyses were performed by a JEOL, JEM-1400 Plus coupled with energy dispersive X-ray spectrometer (EDS), respectively. The composition and phase of P-MoS_2/TiO_2 HM were determined by powder X-ray diffraction (XRD, Rigaku, UltimaIV) using Cu Kα radiation. Raman spectra were recorded at ambient temperature using a Raman spectrometer (inVia Qontor, Renishaw plc) with excitation wavelength (λ = 532 nm). X-ray photoelectron spectroscopy (XPS, ESCALAB 250Xi, UK) analyses were performed on a Thermo VG Scientific using an X-ray monochromator system for the Al K-Alpha irradiations (photon energy 1486.6 eV) under a background pressure (1.0×10^{-9} mbar). The adventitious C1s peak at 284.8 eV was chosen as the calibration reference for XPS spectra. The peak fitting was analyzed using XPS peak fitting software with the Gaussian-Lorentzian function. The background of spectra was subtracted by a Shirley model. And the line shape of different elements combined with 80% Gaussian-Lorentzian value. Besides, the elements P and S 2p 3/2 and 1/2 spin-orbit splitting area ratio value was set to 2 and the elements Mo 3d 5/2 and 3/2 spin-orbit splitting region ratio value was set to 1.5. Fourier transform infrared (FT-IR) spectra were measured using a Nicolet iS10 spectrometer (Nicolet iS50). UV-vis diffuse reflectance spectra (UV-vis DRS) spectra were recorded with a spectrophotometer Shimadzu UV-2600. The Brunauer-Emmett-Teller (BET)

method (Belsorp-max) was used to determine the specific surface area. The thermal stability of sample was performed by thermalgravimetric analyzer (TGA) with DTG-60H analyzer under N_2 atmosphere. The surface wettability was characterized by measuring the static contact angles (CAs) using an optical tensiometer (Attension Theta Lite, Biolin Scientific). Photoluminescence (PL) spectra were measured on a FluoroMax-4 fluorescence spectrophotometer (Shimadzu, RF-6000) with an excitation of 325 nm. Electron paramagnetic resonance (EPR) spectra were conducted on a Bruker EMXplus. The radicals trapping experiments were carried out by adding the different scavengers. And the specific experimental conditions: 1 mmol L^{-1} of 2,4-dichlorophenol (2, 4-DCP) for H*, 0.5 mmol L^{-1} of $AgNO_3$ for photogenerated electrons, 1 mmol L^{-1} of benzoquinone for $\cdot O^{2-}$, 1 mmol L^{-1} of isopropanol for ·OH.

Text S5. Theoretical calculation

In this study, density functional theory (DFT) calculation was performed using the Vienna *ab initio* simulation package, along with spin-polarized PBE-GGA exchange-correlation functional correction and projector augmented wave technique. Convergence criteria for the total energy and atomic force set to 1×10^{-5} eV and 0.03 eV/Å, respectively. The plane wave basis was expanded with an energy cut off of 500 eV. To minimize the interaction between two adjacent layers, the vacuum slab was set as 25 Å. The Gamma-centered Monkhorst-Pack meshes of 5 × 4 × 1 were used for sampling the Brillouin-zone to calculate the band structure and density of states (DOS), and the regular k-point grids of 3 × 2 × 1 were selected for the optimization of structure. Besides, the GGA+U method introduced an inter-atomic interaction as an on-site

correction, which can make the calculation results close to the experimental values. To clarify the correlated interactions bewteen electronic structure and Ti 3d electrons, a moderate on-site coulomb repulsion U = 7.0 eV was employed. Based on the characterization and experimental results, the selection of active sites was screened and optimized during DFT calculation.

The Gibbs free energy change (ΔG) of adsorbate was calculated as follows equation 1:[2]

$$\Delta G = \Delta E_{H^*} + \Delta E_{ZEP} - T\Delta S \quad (1)$$

where ΔE_{H^*}, ΔE_{ZEP} and ΔS are adsorption energies, zero-point energy correction, and entropy change of the hydrogen atom after adsorbing on the surface, respectively. As the vibrational entropy of H* adsorption is small, the 1/2 entropy change of H_2 in the adsorbed state approximates in the gas-phase under standard conditions. Hence, the correction can be taken as: $\Delta G_{H^*} = \Delta E_{H^*} + 0.24$ eV, and ΔE_{H^*} is calculated as equation 2:

$$\Delta E_{H^*} = E_{total} - E_{sur} - 1/2\, E_{H_2} \quad (2)$$

where E_{total}, E_{sur} and E_{H_2} represent the total energy of the adsorption system, energy of pure surface, and the energy of H_2 molecule in a vacuum, respectively.

The adsorption energy change ($\Delta E_{Cr(VI)}$) of Cr (VI) is defined as equation 3:

$$\Delta E_{Cr(VI)} = E_{close} - E_{away} \quad (3)$$

where E_{close} and E_{away} represent the total energy of the adsorption system when Cr (VI) is close to (~1.5 Å) or away from (> 6 Å) the surface (Fig. S2). The structural

models of samples are presented as follow (1-2):

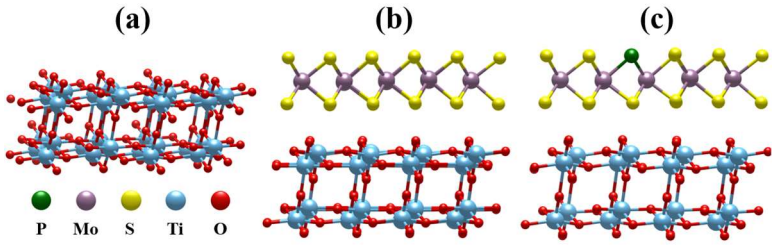

(1) Surface structure of (a) TiO_2 HM, (b) MoS_2/TiO_2 HM, and (c) P-MoS_2/TiO_2 HM.

$$\Delta E_{Cr(VI)} = E_{close} - E_{away}$$

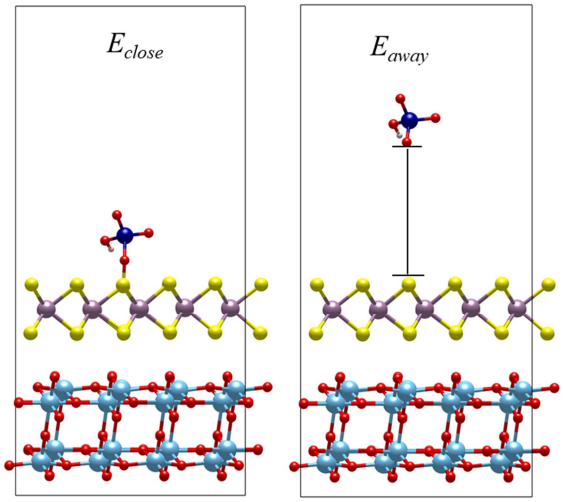

(2) The schematic diagram of calculating adsorption energy change of Cr (VI) on a given surface.

FIGURES

Fig. S1. The color change of as-prepared samples

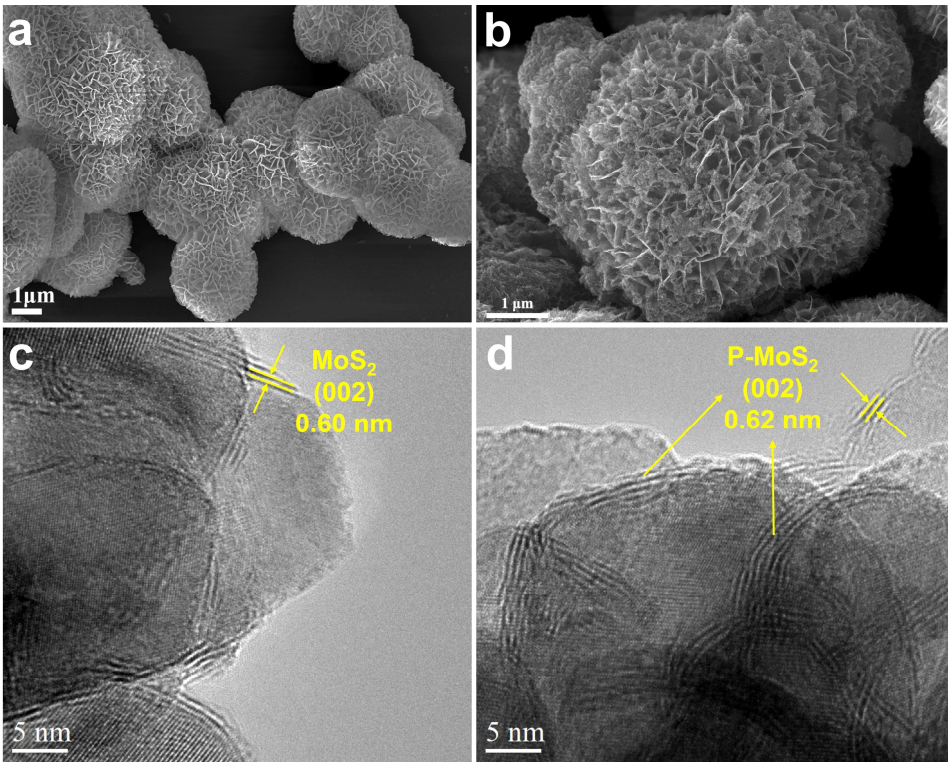

Fig. S2. SEM and TEM images

SEM images of (a) TiO_2 HM and (b) P-MoS_2/TiO_2 HM samples; TEM images of (c) MoS_2/TiO_2 HM and (d) P-MoS_2/TiO_2 HM samples.

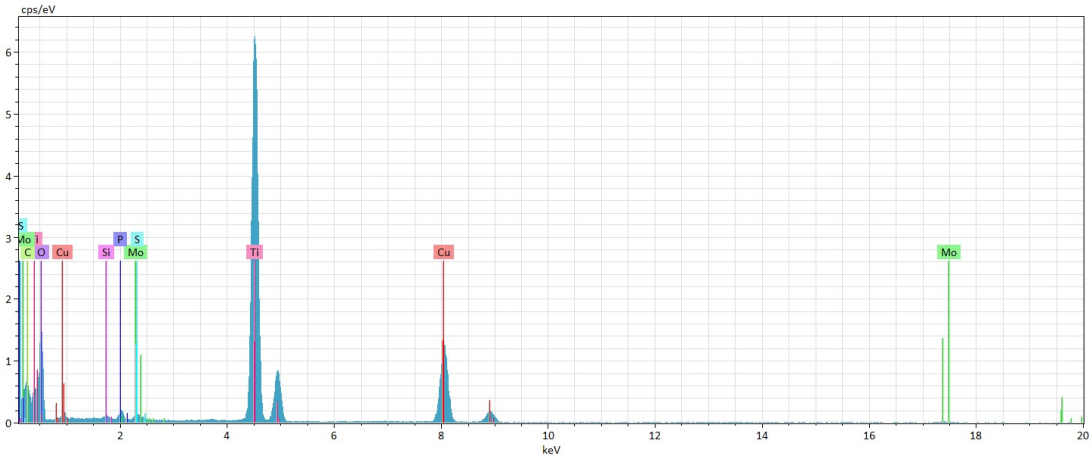

Fig. S3. EDS pattern of P-MoS_2/TiO_2 HM

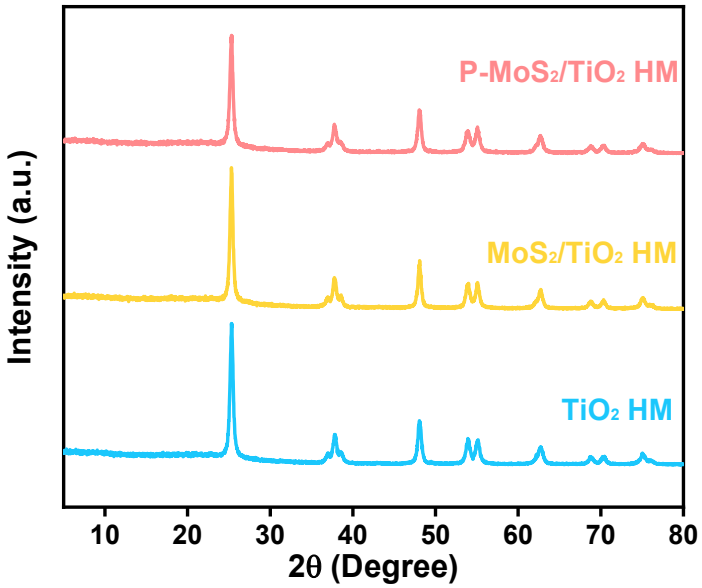

Fig. S4. XRD pattern of as-prepared samples

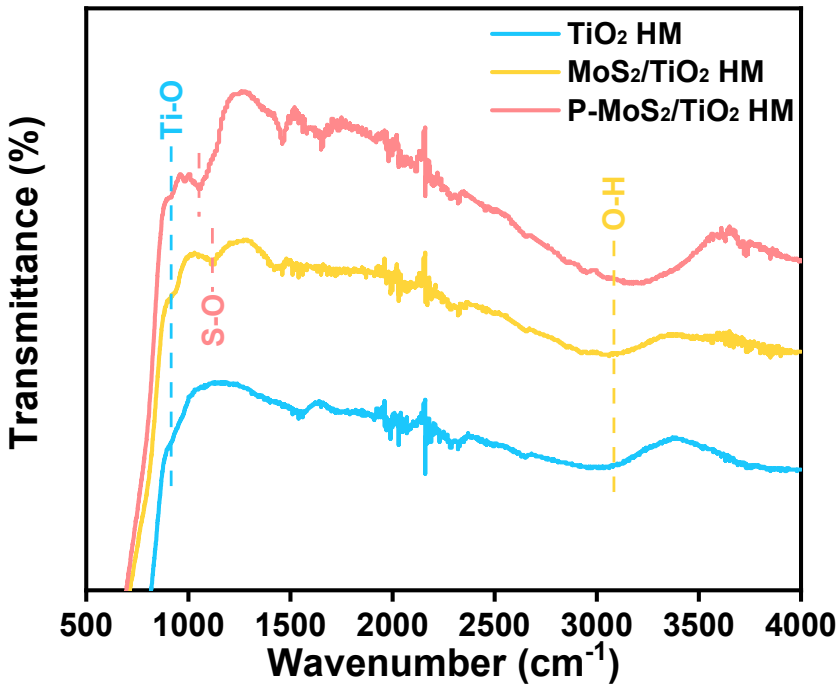

Fig. S5. FT-IR spectra of as-prepared samples

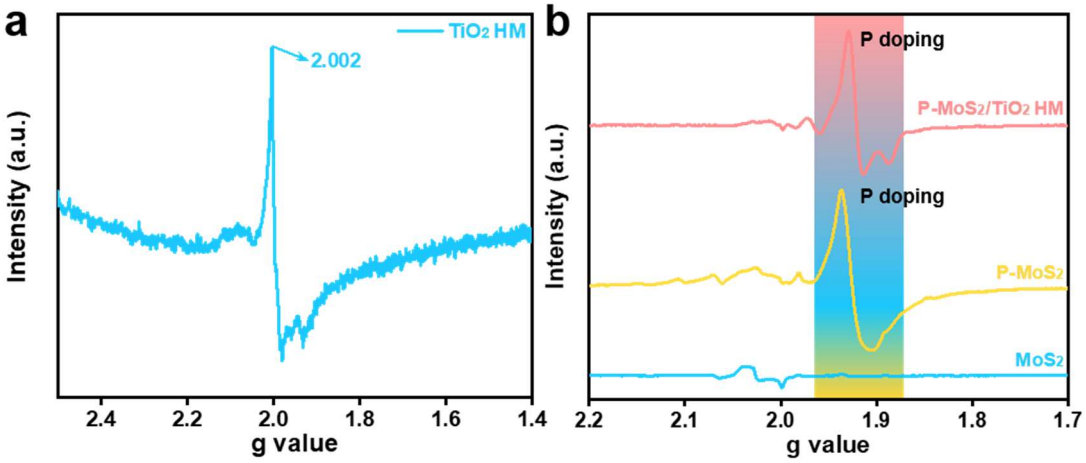

Fig. S6. EPR spectra of as-prepared samples

EPR spectra of (a) TiO_2 HM, (b) MoS_2, P-MoS_2, P-MoS_2/TiO_2 HM.

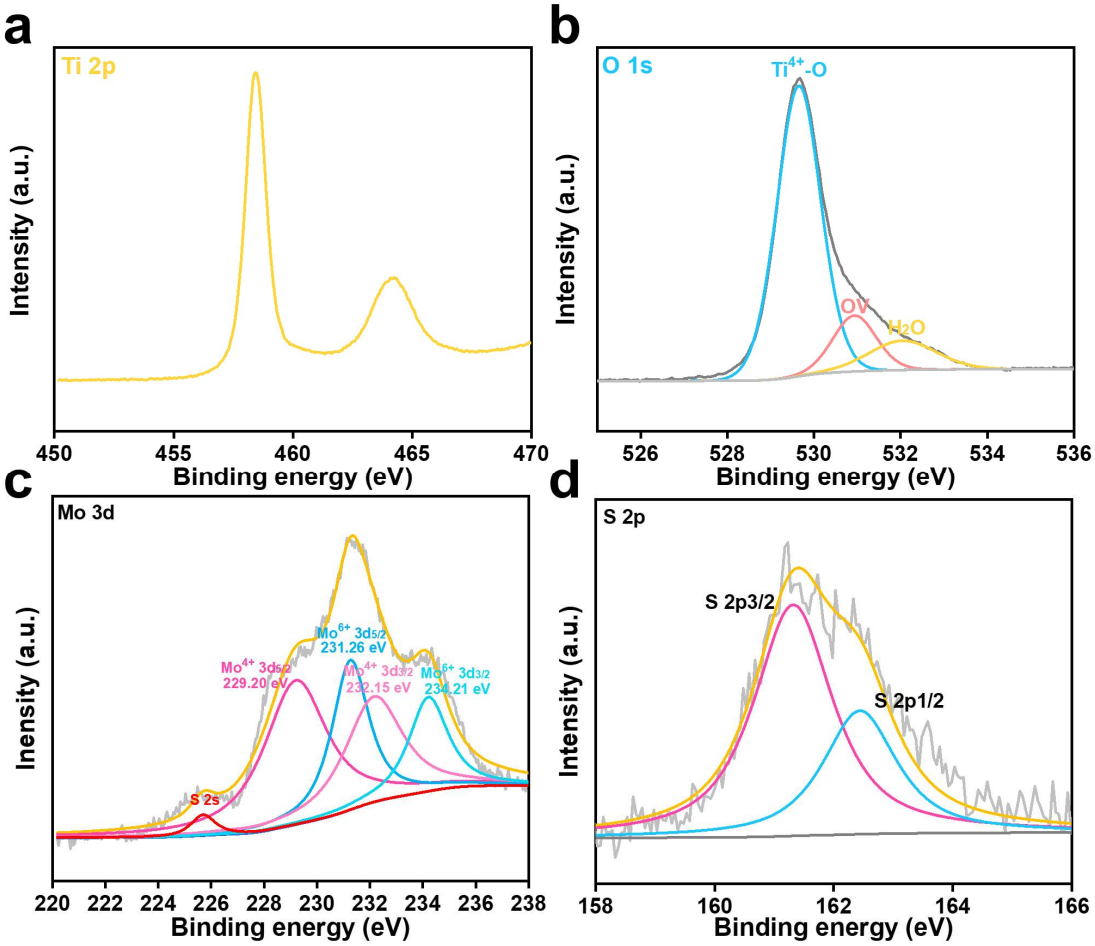

Fig. S7. High-resolution XPS spectrum of P-MoS_2/TiO_2 HM sample

High-resolution XPS spectrum of P-MoS_2/TiO_2 HM sample: (a) Ti 2p, (b) O 1s, (c) Mo 3d and (d) S 2p.

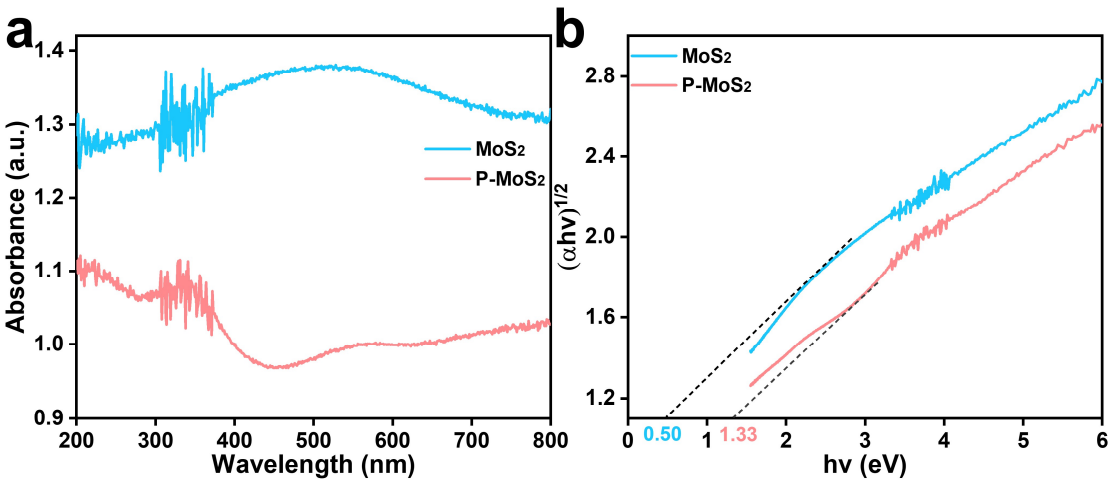

Fig. S8. UV-Vis DRS and the corresponding Tauc plots

(a) UV-Vis DRS and (b) the corresponding Tauc plots of $(\alpha h\nu)^{1/2}$ versus hν of MoS_2 and P-MoS_2 samples.

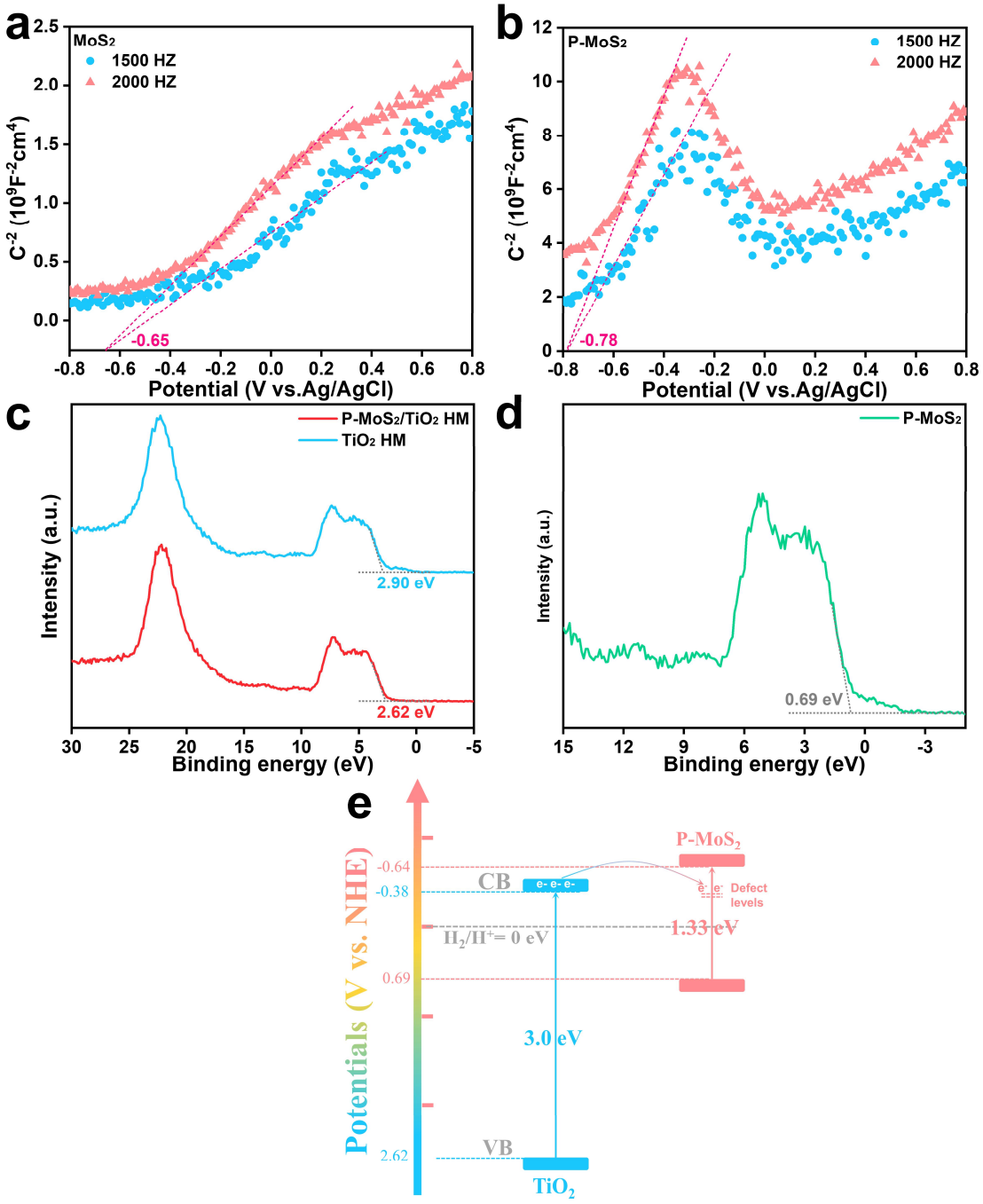

Fig. S9. Mott-Schottky plots, XPS-valance band (VB) spectra and the band alignment

Mott-Schottky plots of (a) MoS_2 and (b) P-MoS_2; (c-d) XPS-VB spectra of TiO_2, P-MoS_2/TiO_2 HM and P-MoS_2; (e) The band alignment of P-MoS_2/TiO_2 HM.

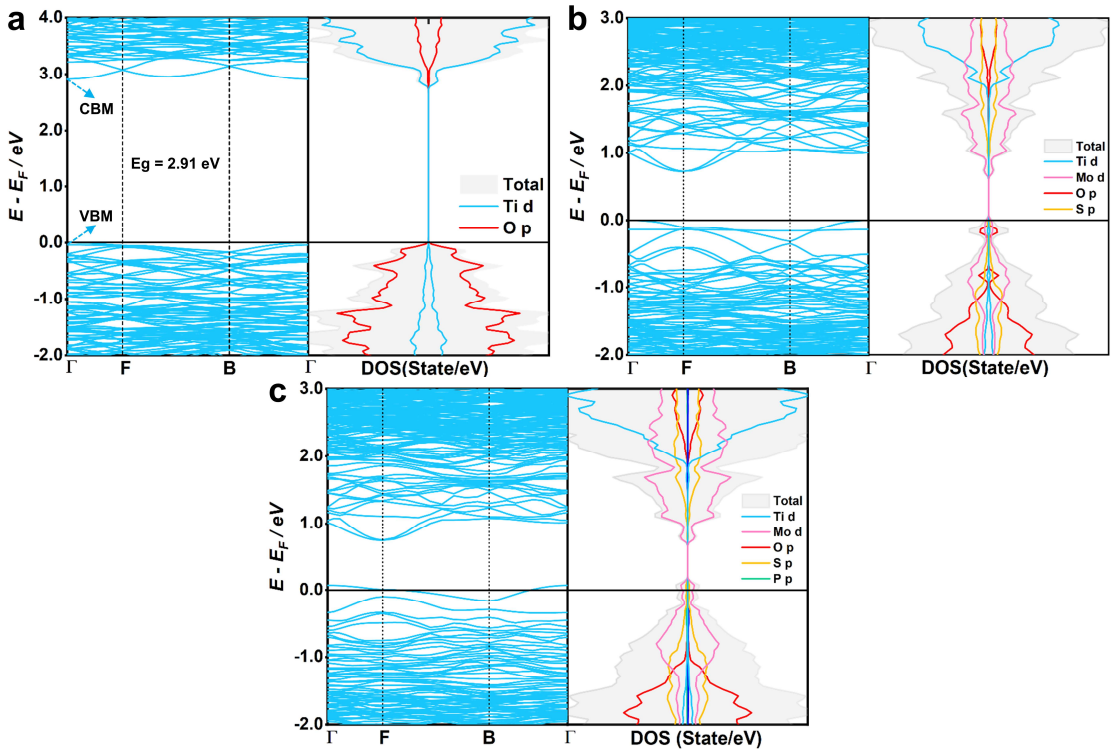

Fig. S10. Energy band structure and density of states of different materials

Energy band structure and density of states of (a) TiO_2 HM, (b) MoS_2/TiO_2 HM and (c) P-MoS_2/TiO_2 HM.

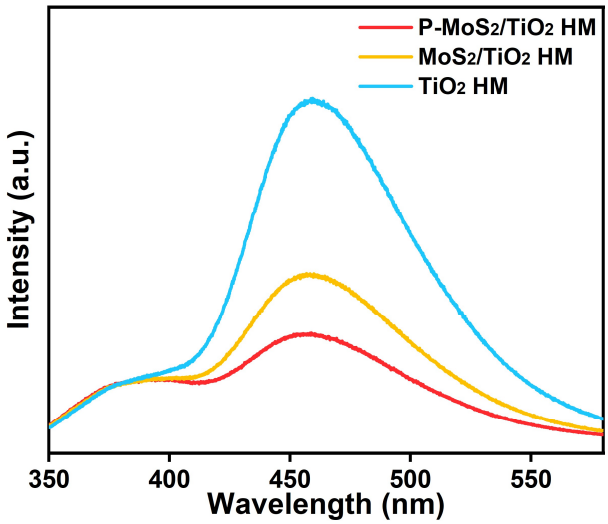

Fig. S11. Steady state PL spectra of as-prepared samples

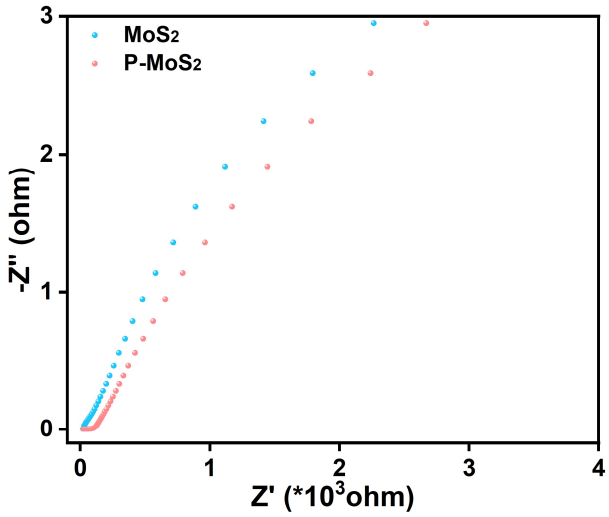

Fig. S12. EIS plots of as-prepared samples

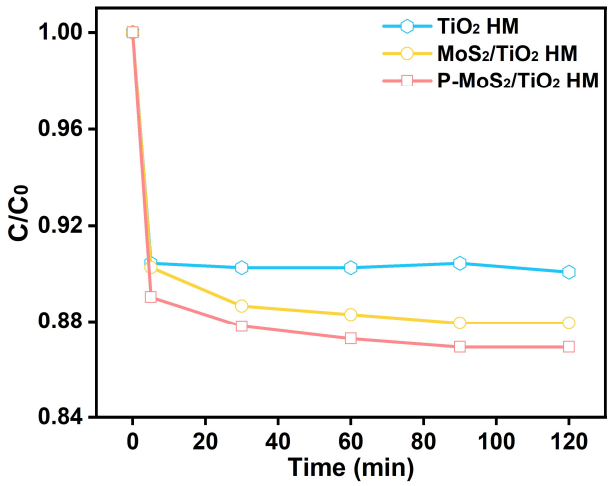

Fig. S13. Adsorption-desorption equilibrium curves of Cr (VI) over different catalysts (pH = 3).

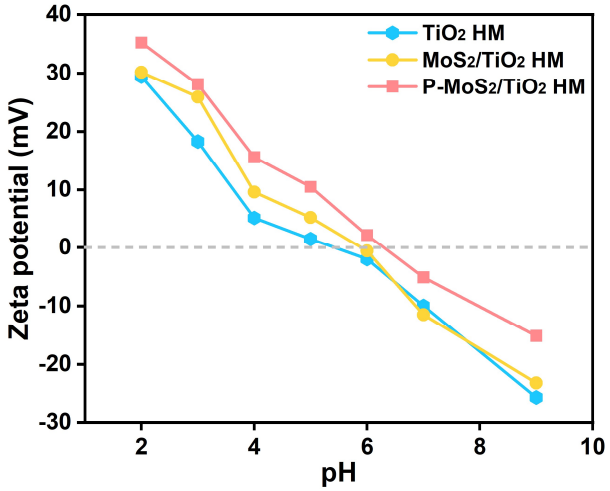

Fig. S14. The zeta potential of as-prepared materials.

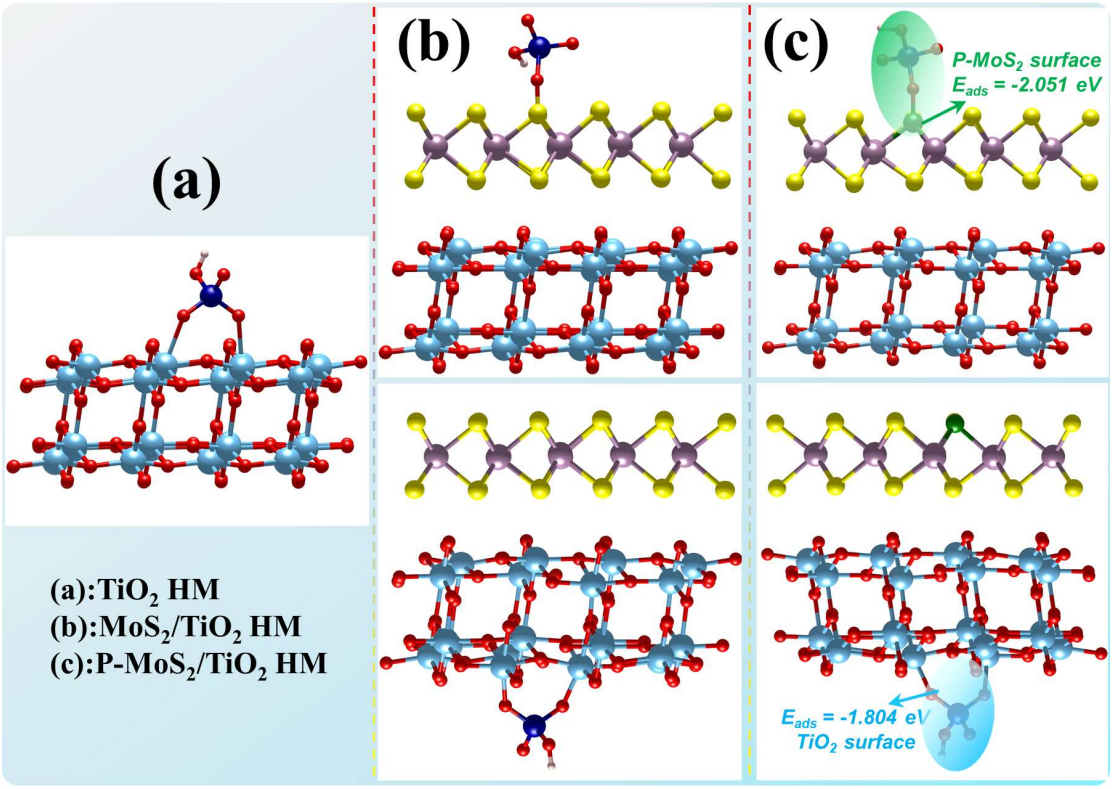

Fig. S15. The adsorption model of Cr (VI) ions on the different materials surface

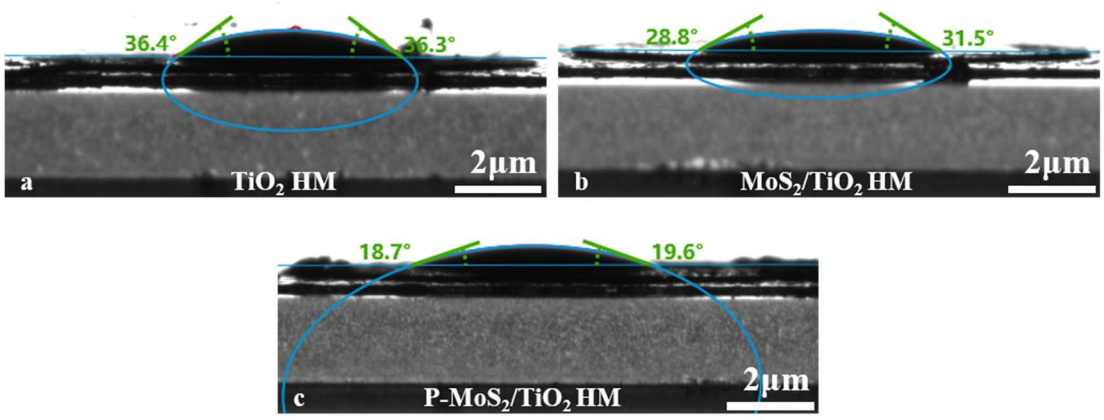

Fig. S16. Contact angle measurements

The images showing contact angles of water droplets on (a) TiO_2 HM, (b) MoS_2/TiO_2 HM and (c) P-MoS_2/TiO_2 HM samples.

Table S1. Primary properties of water samples

Parameter	Unit	Tap water	WWTP effluent water	Seawater
pH	/	7.57	6.93	8.17
TOC	mg/L	1.42	4.31	0.23
Cl^-	ppm	10.77	58.61	18451.87
HCO_3^-	ppm	3.81	2.77	5.46
SO_4^{2-}	ppm	17.28	46.72	2541.96
Na^+	ppm	11.57	36.91	10100
K^+	ppm	3.48	10.59	374

Table S2. The adsorption energy of Cr (VI) ions on the different materials surface

Samples	E_{ads}	
	$TiO_{2\ surface}$	$MoS_{2\ surface}$
TiO_2 HM	-0.992	/
MoS_2/TiO_2 HM	-1.844	-0.398
P-MoS_2/TiO_2 HM	-1.804	-2.051

Table S3. Reports on the dual-functional proposes for photocatalytic H_2 evolution and Cr (VI) reduction in recent literatures.

Catalyst	Light source	Evolved H_2 rate	Degradation rate	Year[Ref]
P-MoS_2/TiO_2 HM	Full spectrum	1550.30 μmol $g^{-1}h^{-1}$	100%	Our work
CuO/g-C_3N_5	Full spectrum	37.4 μmol/4h	92%	2023[3]
Pt/Co@NC/CdSe	λ > 400 nm	6.48 mmol $g^{-1}h^{-1}$	99.5%	2023[4]
Pt/g-C_3N_4(TCPs)	>420 nm	1919.0 μmo l $g^{-1}h^{-1}$	95.8%	2023[5]
CeO_2/CdS	λ > 420 nm	751.3μmmo l $g^{-1}h^{-1}$	99.94%	2022[6]
Pt/CCCN	Full spectrum	4207 μmol $g^{-1}h^{-1}$	96.7%	2022[7]
Fe_3O_4@UiO-66	Full spectrum	417 μmol h^{-1}	99.82%	2022[8]
$MoSe_2$/ $Zn_{0.5}Cd_{0.5}S$	λ > 420 nm	4853.3 μmol $g^{-1}h^{-1}$	98%	2021[9]
$SnIn_4S_8$/CeO_2	λ > 420 nm	619.3μmmo l $g^{-1}h^{-1}$	98.8%	2021[10]
$ZnIn_2S_4$/MoS_2	λ > 420 nm	200.1 μmol $g^{-1}h^{-1}$	82.8%	2020[11]
P/Mo/g-C_3N_4	λ > 420 nm	118 μmol h^{-1} g^{-1}	95%	2019[12]

Table S4. The specific values of contact angle measurement

Sample	Contact Angle
TiO_2 HM	36.4°
MoS_2/TiO_2 HM	31.2°
P-MoS_2/TiO_2 HM	19.2°

References:

1. D. Zhang, C. Lee, H. Javed, P. Yu, J.-H. Kim and P. J. J. Alvarez, *Environmental Science & Technology*, 2018, **52**, 12402-12411.
2. J. K. Noerskov, T. Bligaard, A. Logadottir, J. R. Kitchin, J. G. Chen, S. Pandelov and U. Stimming, *ChemInform*, 2005, **36**.
3. R. Sethy, S. R. Torati, A. Panigrahi, B. Nanda, P. Pattnaik and B. Naik, *Inorganic Chemistry Communications*, 2023, **157**, 111294.
4. M. Chen, H. Fang, C. Wang, J. Xu and L. Wang, *Journal of the Taiwan Institute of Chemical Engineers*, 2023, **146**, 104798.
5. Z. Jin, S. Jin, S. li, R. Zou, D. Wang, F. Dong, M. Liu, S. Song and T. Zeng, *Journal of Cleaner Production*, 2023, **422**, 138556.
6. H. Yin, C. Yuan, H. Lv, X. Chen, K. Zhang and Y. Zhang, *Separation and Purification Technology*, 2022, **295**, 121294.
7. X. Chen, X. Li, L. Song, R. Chen, H. Li, J. Ding, H. Wan and G. Guan, *International Journal of Hydrogen Energy*, 2022, **47**, 20803-20815.
8. S. Prakash Tripathy, S. Subudhi, S. Das, M. Kumar Ghosh, M. Das, R. Acharya, R. Acharya and K. Parida, *Journal of Colloid and Interface Science*, 2022, **606**, 353-366.
9. Y. Jia, Z. Wang, X.-Q. Qiao, L. Huang, S. Gan, D. Hou and D.-S. Li, *Applied Surface Science*, 2021, **554**, 149649.
10. C.-H. Shen, Y. Chen, X.-J. Xu, X.-Y. Li, X.-J. Wen, Z.-T. Liu, R. Xing, H. Guo and Z.-H. Fei, *Journal of Hazardous Materials*, 2021, **416**, 126217.
11. W. Pudkon, H. Bahruji, P. J. Miedziak, T. E. Davies, D. J. Morgan, S. Pattisson, S. Kaowphong and G. J. Hutchings, *Catalysis Science & Technology*, 2020, **10**, 2838-2854.
12. D. Chen, J. Liu, Z. Jia, J. Fang, F. Yang, Y. Tang, K. Wu, Z. Liu and Z. Fang, *Journal of Hazardous Materials*, 2019, **361**, 294-304.